Environ. Sci. Technol. **1998**, *32,* 2931−2939

Biogeochemical Cycles of Manganese and Iron at the Oxic−Anoxic Transition of a Stratified Marine Basin (Orca Basin, Gulf of Mexico)

PHILIPPE VAN CAPPELLEN,* ERIC VIOLLIER,‡ AND ALAKENDRA ROYCHOUDHURY

School of Earth and Atmospheric Sciences, Georgia Institute of Technology, Atlanta, Georgia 30332-0340

LAUREN CLARK AND ELLERY INGALL

Marine Science Institute, University of Texas at Austin, Port Aransas, Texas 78373-1267

KRISTINE LOWE AND THOMAS DICHRISTINA

School of Biology, Georgia Institute of Technology, Atlanta, Georgia 30332-0230

Chemical distributions and microbial culture data are combined to identify the biogeochemical pathways that control the cycles of manganese and iron at the oxic−anoxic transition of the Orca Basin. The redox transition coincides with an increase in salinity from 35 to 260‰; hence, mixing diagrams are used to constrain the salinity ranges over which consumption or production of solute species takes place. Analysis shows that the very high dissolved Mn(II) levels (>400 μM) at intermediate salinities (60−180‰) result from dissimilatory (microbial) reduction of manganese oxides, coupled to organic matter oxidation. The manganese oxides are continuously regenerated in the oxygenated, low-salinity region (45−52‰) by microbial oxidation of dissolved Mn(II). Precipitation of manganese carbonate in the high-salinity zone (>180‰) is the main removal mechanism of Mn to the sediments. Upward diffusing Fe(II) ions are extracted from solution within the anoxic, high-salinity range (230−260‰), through anaerobic oxidation by manganese oxides or a nonoxidative sorption process. Ferric oxyhydroxides are reduced by reaction with dissolved sulfide and are, therefore, not an important terminal electron acceptor for organic matter oxidation. Overall, the acid−base chemistry, redox transformations, and microbial activity across the salinity transition are strongly coupled to the cycle of manganese.

Introduction

The behavior of iron and manganese at oxic to anoxic transitions is generally assumed to be driven by redox reactions (*1*). Under oxic conditions insoluble solid oxyhydroxides of Fe and Mn are produced by oxidative precipitation, whereas under anoxic conditions the reductive dissolution of the oxyhydroxide phases regenerates Fe(II) and Mn(II). Redox cycling of Fe and Mn occurs when opposite transport fluxes move the reduced and oxidized species to the oxic and anoxic portions of the system, respectively. Such cycling has been reported in water columns (*2*), sediments (*3, 4*), and groundwater environments (*5*).

Reduction and oxidation of Fe and Mn, however, may proceed through a wide variety of biogeochemical pathways, including homogeneous, mineral surface-controlled, photochemical, and enzymatically mediated electron-transfer reactions (*6*−*8*), whereas many nonredox reactions also affect the speciation and, hence, the fate of the metals (*1, 5*). Therefore, in any given environmental setting, an important task is to determine which particular set of reaction pathways controls the cycles of the two elements.

The oxic to anoxic transition in the Orca Basin coincides with an increase in salinity from 35 to 260‰. Large changes in the concentrations of dissolved and particulate Mn and Fe are observed across the salinity transition zone. These have been interpreted in terms of redox cycling of the metals, with dissolved Mn(II) and Fe(II) moving up toward the oxygenated waters and oxyhydroxide phases settling in the opposite direction (*9*). However, the actual biogeochemical processes involved are not well-constrained.

Here, we combine chemical measurements and microbial culture data to construct a more detailed picture of the biogeochemical cycles of Fe and Mn in the stratified water column of the Orca Basin. Our objective is to identify, among the many potential pathways, those chemical and microbial processes that explain the observed distributions of manganese and iron in this marine environment.

Study Site

The Orca Basin is a bathymetric depression on the northern slope of the Gulf of Mexico, off the coast of Louisiana (Figure 1). It covers ~400 km^2. The maximum water depth lies ~600 m below the surrounding sea floor (*10*). The origin of the depression is related to regional salt tectonics. Nearby salt deposits are also the source of the brine that fills the lower 180 m of the basin (Figure 2A). The brine has a salinity ~7.5 times higher than that of normal seawater.

The large density gradient creates a strong stratification of the seawater−brine interface, as shown by the dramatic increase of the Brunt−Väisälä frequency (*11*) in the depth range from 2230 to 2243 m (Figure 2B). Within this depth zone, vertical turbulent motion is suppressed, hence limiting vertical solute exchanges between the brine and the overlying seawater. As a consequence, the brine pool remains permanently anoxic.

A large fraction of the particulate matter settling into the basin is trapped within the high-density waters of the salinity transition region (*12*). This results in a pronounced maximum of the particulate load. Trefry et al. (*9*) observed that the total concentration of suspended matter within the zone of most stable stratification increases up to 880 μg L^{-1}, compared to 20−60 μg L^{-1} above 2100 m and 200−400 μg L^{-1} below 2250 m. They also report that particles trapped in the salinity transition zone contain up to 60% organic matter.

The Orca Basin was discovered in the 1970s (*10*). Although there have been only a limited number of studies of the water column chemistry, the existing data indicate that the depth profiles of temperature, salinity, and other physicochemical parameters measured at similar locations have not changed

* Corresponding author phone: (404)894-3883; fax: (404)894-5638; e-mail: pvc@eas.gatech.edu.

‡ Present address: Laboratoire de Géochimie des Eaux, Université Denis-Diderot-Paris 7, 2 Place Jussieu, 75251 Paris Cedex 05, France.

S0013-936X(98)00307-1 CCC: $15.00
Published on Web 08/21/1998

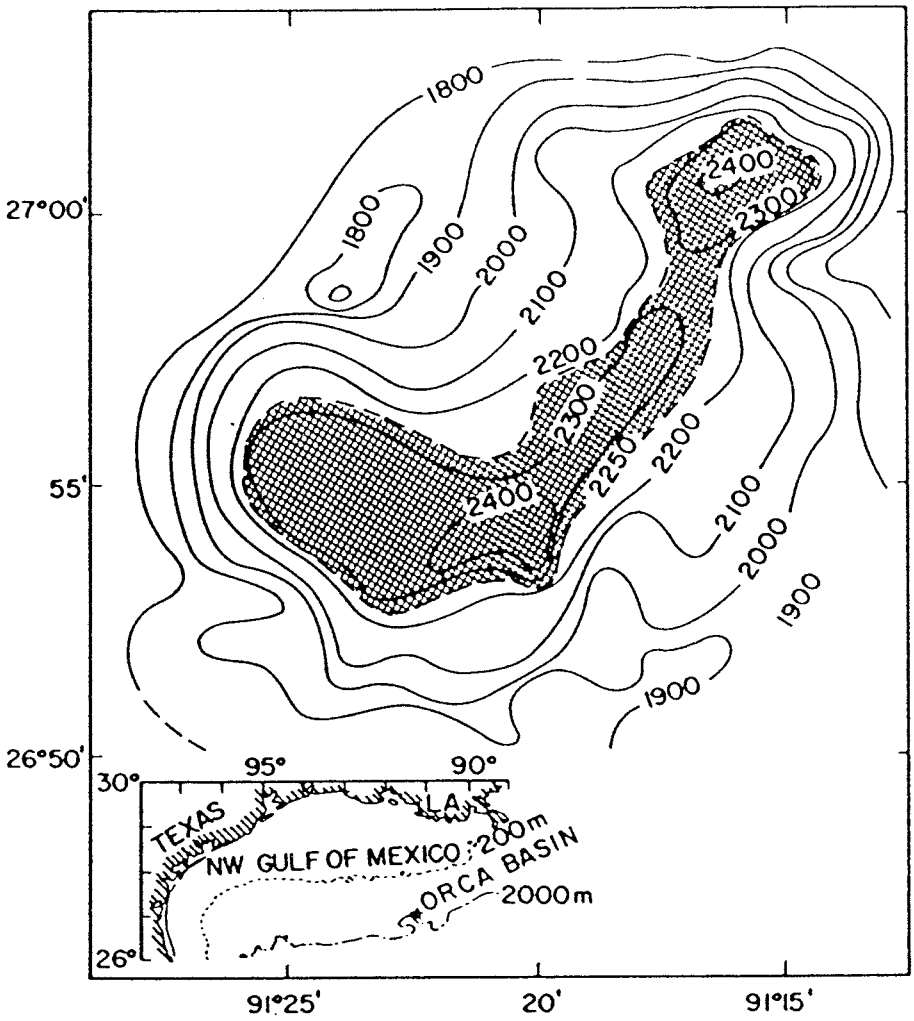

FIGURE 1. Location and bathymetry of the Orca Basin (from ref *10*). Stippled area corresponds to the portion of the basin filled with brine. Data presented in this paper are from the deepest part of the southern sub-basin.

significantly between the earliest studies and our recent cruises (*9*, *10*, *12*−*14*). Thus, on a decadal time scale, the water column chemistry of the Orca Basin appears to remain close to steady state.

Sampling and Methods

Data presented here are from the central part of the larger southern sub-basin (Figure 1). Water samples were collected during three cruises of the R/V *Longhorn*, April 22−30, 1996 (ORCA I), September 4−12, 1996 (ORCA II), and November 8−16, 1996 (ORCA III), using 12 L Niskin bottles mounted on a CTD rosette. Temperature, dissolved oxygen, and conductivity were directly recorded by the CTD probes. The brine, however, falls outside the CTD conductivity range, and additional conductivity measurements were made with a portable conductivity meter on diluted (1:21) water samples. The measurements were made at room temperature and calibrated with a seawater standard at the same temperature.

Polypropylene syringes were used to retrieve water from the outlets of the Niskin bottles. The samples were filtered immediately through in-line 0.4 μm pore size polypropylene membranes (Whatman). The syringe−filter assemblage was connected to a flow-through pH electrode. Sample was then injected in the electrode chamber, and pH was recorded under no-flow conditions. After the pH was measured, filtrate was distributed among vials containing specific reagents for spectrophotometric measurements or sample preservation. All shipboard determinations of redox-sensitive parameters were performed within hours of sample collection.

The pH electrode was calibrated with artificial seawater−Tris buffer (*15*). Salinity variations across the seawater−brine interface modify the liquid junction potential of the electrode and hence may lead to errors in the absolute pH determinations. To constrain the potential magnitude of the errors, we used the pH and alkalinity measurements to calculate total dissolved CO_2 concentrations in the brine. The calculated values were then compared to the direct $\sum CO_2$ measurements by Wiesenburg (*13*). Reasonable agreement was observed, indicating that liquid junction effects cause only a relatively small bias in the absolute pH values (<0.1 pH unit), in agreement with previous work (*13*, *16*).

Alkalinity was determined spectrophotometrically using a bromophenol blue colorometric method (*17*). Dissolved Fe(II) was measured using the ferrozine method (*18*), with an added hydroxylamine reduction step to separate the contributions of Fe(II) and Fe(III) to total dissolved iron. Total dissolved sulfide was trapped in a ZnCl gelatine medium and then analyzed according to the standard methylene blue method. Nitrate, ammonium, and dissolved manganese were determined according to standard seawater analysis methods (*19*, *20*), adapted for high-salinity samples. When needed, salinity adjustments of samples, blanks, and standards were done using a degassed NaCl solution.

Particulate matter was collected on 0.4 μm pore size polycarbonate membranes (Nucleopore) by N_2-pressure

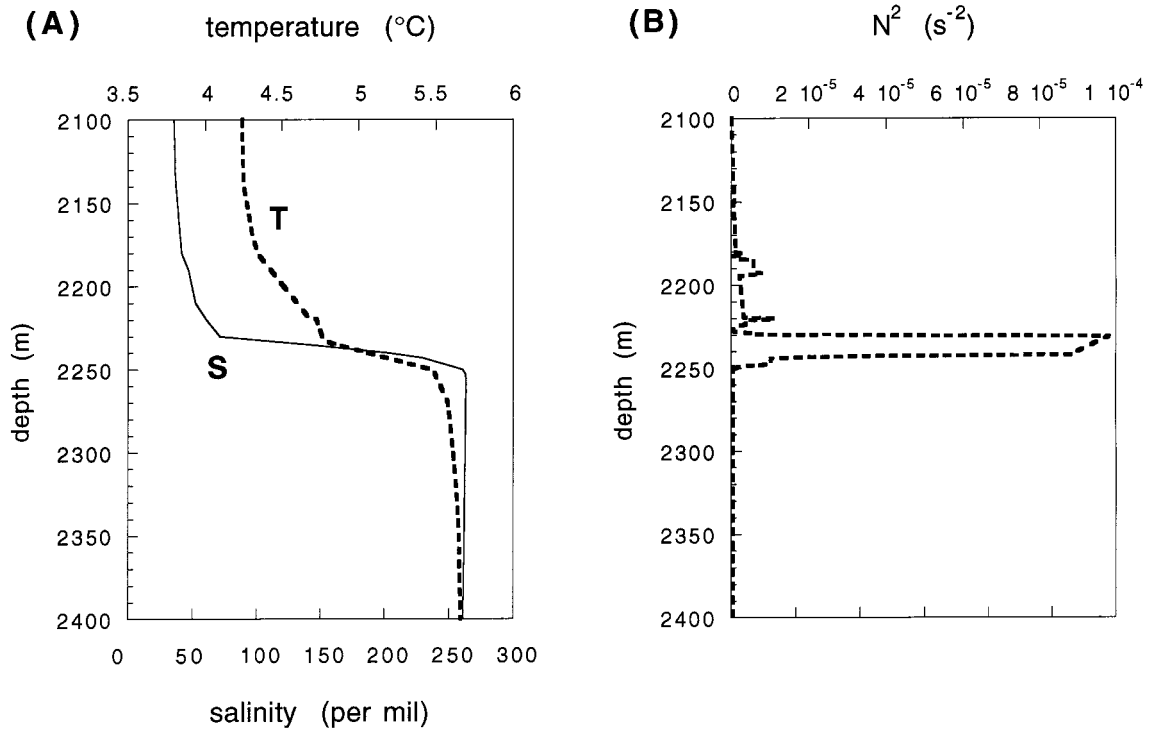

FIGURE 2. Depth profiles of temperature, salinity (A), and the square of the Brunt−Väisälä frequency, N^2 (B), across the seawater to brine transition. N^2 is a measure of the stability of stratification (*11*); the vertical eddy diffusivity correlates inversely with N^2.

filtration of 1−2 L of water. The membranes were subsequently attacked with bidistilled nitric acid (Optima, 1 M) at 80 °C, for 1 week. Total Fe in solution was determined using the ferrozine method; total manganese was measured by ICP-MS.

For enumeration of bacterial numbers, a subset of unfiltered water samples from the November 1996 (ORCA III) cruise were spread on solid agar medium containing various combinations of carbon/energy sources and terminal electron acceptors. Aerobic bacteria were enumerated by duplicate plating on either complex (nutrient agar; Difco, Detroit, MI) or defined (*21*) growth medium supplemented with lactate (15 mM) or acetate (10 mM) as sole carbon/energy source. Anaerobic Fe(III)-reducing (FRB) and Mn(IV)-reducing bacteria (MRB) were enumerated by duplicate plating on analogous growth media supplemented with either Fe(III)−citrate (50 mM) or MnO_2 (1 mM) as sole terminal electron acceptor (*22*). Fe(II)-oxidizing (FOB) and Mn(II)-oxidizing bacteria (MOB) were enumerated by duplicate plating on B1 medium (*24*) supplemented with either $FeSO_4$ or $MnSO_4$ (both at 0.002%, w/v) as sole energy source. All medium preparations were supplemented with NaCl to a final concentration of 35‰.

FRB and MRB incubations were carried out under anaerobic conditions in airtight glass containers, using the GasPak Plus anaerobic generating system (Becton Dickinson Co., Cockeysville, MD). FOB and MOB incubations were carried out under microaerobic conditions (5−10% O_2) in identical containers, using the CampyPak Plus microaerobic generating system (Becton Dickinson Co.). All incubations were carried out in the dark for 1 month at 4 °C, followed by 3 months at room temperature before plates were scored for bacterial colonies (colony forming units, CFU) and the production of clearing zones (FRB, MRB) or oxidized, particulate forms of Fe and Mn (FOB, MOB). To ensure that a strict anaerobic or microaerobic atmosphere was maintained throughout the incubation period, control plates were included in each glass container. The control plates consisted of analogous growth media with either the carbon/energy source or terminal electron acceptor omitted. CFU were never observed on the control plates, indicating that strict growth conditions were maintained throughout the incubation period.

Results and Discussion

Production and consumption of chemical species in a water column are often inferred from the concentration depth profiles. A concentration decrease (increase) with depth is interpreted as reflecting consumption (production) of the species by a chemical or biological process. This simple interpretation of water column concentration gradients assumes that the profiles are not significantly affected by lateral transport or by non-steady-state effects. In addition, it implicitly assumes that transport properties in the water column do not change appreciably over the depth range of interest. If this is not the case, then changes in the concentration gradient with depth will partly reflect variations in the transport parameters.

One way to eliminate the effects of variable vertical eddy diffusivity on the concentration distributions of solutes in the transition zone is to plot the concentrations versus salinity, in a so-called mixing diagram. In such a diagram, the concentrations of a conservative (nonreactive) dissolved species lie on a straight line between the end-member seawater and brine concentrations. Alternatively, when the plot shows curvature, it indicates either production (concave-up) or consumption (convex-down). Such mixing diagrams are routinely used to interpret chemical distributions in estuaries (*25*).

The depth distribution of ammonium (Figure 3) illustrates that the interpretation of concentration versus depth profiles in the stratified portion of the Orca Basin may not be straightforward. At first sight, the large increase in concentration between 2220 and 2245 m may lead one to infer a high rate of production of ammonia within this depth range. However, when plotted against salinity, the ammonium concentration follows a near-linear trend in the corresponding salinity range, 60−245‰ (Figure 4A). Therefore, the

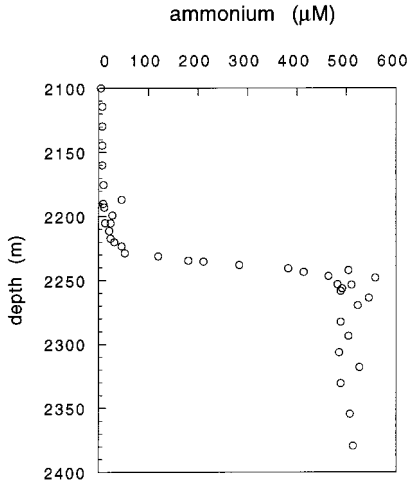

FIGURE 3. Depth profile of ammonium.

distribution of ammonium in the region above the brine primarily reflects conservative mixing of the ammonium-enriched brine with seawater.

In what follows, we will use mixing diagrams to constrain the salinity ranges, and therefore the depth ranges, over which net consumption or production of dissolved species occurs. For example, removal of molecular oxygen is restricted to the low-salinity range (<70‰) of the transition zone (Figure 4B). For dissolved O_2, the interpretation of the mixing diagram is straightforward, because O_2 is consumed but not produced. More complex situations may be encountered when both removal and production processes take place, for example, in the case of dissolved Mn(II) or Fe(II) (see below). The interpretation of solute mixing diagrams given in this paper assumes only two end-members, which is equivalent to assuming that the concentration distributions are not influenced by lateral inputs or outputs. This is obviously an oversimplification because the sediments along the margins of the basin may (and probably do) act as sources or sinks of dissolved and particulate species.

The decrease of particulate settling velocities, and consequently the increased residence time of organic-rich particles in the transition zone, promotes extensive oxidative degradation of organic matter by bacteria. Furthermore, restricted solute transport limits the downward resupply of dissolved O_2. Hence, anaerobic pathways must be primarily responsible for the oxidation of organic matter below a depth of 2200 m. This is corroborated by the finding that the CFU counts of aerobic bacteria (data not shown) decline to extremely low levels (none detected, or at the most 10 ± 10 CFU/mL on complex medium) at a sampling depth of 2170 m and below, compared to the high counts ($\sim$4000 $\pm$ 1250 CFU/mL on complex medium) in the waters above 2170 m. Because no NO_3^- persists at salinities above 60‰ (not shown), microbial nitrate reduction, or denitrification, is also limited to depths above 2200 m.

Below 2200 m, manganese and iron oxide phases are the energetically most favorable terminal electron acceptors for the heterotrophic bacteria (*1*). The CFU counts of iron-reducing (FRB) and manganese-reducing bacteria (MRB) remain fairly constant from the sea surface to a depth of 2170 m, but they increase dramatically (30−60-fold) between the sampling depths of 2170 and 2225 m (Figure 5A). The large increase in FRB and MRB CFU suggests that a significant fraction of the heterotrophic population residing between the depth at which O_2 becomes limiting and the top of the brine is capable of respiring anaerobically on either Mn(IV) or Fe(III) as sole terminal electron acceptor.

The dramatic increase in FRB and MRB CFU between depths of 2170 and 2225 m is also observed on defined growth medium with lactate as the sole carbon/energy source (data not shown). The maximum FRB and MRB CFU, however, are $\sim$2−3-fold lower than those observed on complex medium. This reflects most likely a requirement for an unidentified growth substrate (e.g., a carbon source or vitamin) that is not provided in the defined growth medium. Furthermore, the heterotrophic population prefers lactate over acetate as the carbon source: acetate-grown CFU were detected at extremely low levels in all water samples, regardless of depth.

Alkalinity can be used as a tracer of pathways of organic matter breakdown (*1*). Aerobic respiration produces little or no change in alkalinity, whereas anaerobic respiration increases alkalinity. Per unit carbon oxidized, dissimilatory Mn reduction and dissimilatory Fe reduction are the pathways generating the highest amounts of alkalinity. Thus, the large production of alkalinity observed in the intermediate salinity range 60−180‰ (Figure 4C) is consistent with the utilization of manganese or iron oxide phases as terminal electron acceptors for bacterial respiration in the depth range of 2200−2240 m.

The concave-up curvature of the mixing diagram of dissolved Mn^{2+} provides conclusive evidence for reductive dissolution of manganese oxide phases in the intermediate-salinity range (Figure 4D). Both the alkalinity and Mn^{2+} mixing diagrams reach their maximum deviation from the conservative mixing lines at salinities around 150‰. The vertical arrows in Figures 4C,D further show that, on a molar basis, the maximum excess alkalinity is about twice that of Mn^{2+}. This agrees with the alkalinity to Mn^{2+} ratio expected for stoichiometric oxidation of organic matter by MnO_2:

$$CH_2O + 2MnO_2 + 4H^+ \rightarrow 2Mn^{2+} + H_2CO_3 + 2H_2O \quad (1)$$

A 2:1 ratio is also obtained when alternative manganese oxide phases, for example, manganite (MnOOH) or hausmannite (Mn_3O_4), are substituted for MnO_2 in the above reaction. Only slight deviations from the 2:1 ratio in reaction 1 occur when more complete chemical representations of biodegradable marine organic matter are used (*1*).

The lack of curvature in the mixing diagram of Fe(II) between the seawater end-member and a salinity of 230‰ (Figure 4F) argues against reductive dissolution of iron oxides at intermediate salinities, despite the high FRB CFU counts in this region (Figure 5A). One possible explanation for the similarity between the distributions of MRB and FRB CFU is that the same set of bacteria is capable of utilizing both oxidized Mn and Fe as terminal electron acceptor. However, within the intermediate-salinity range, only manganese oxides are being used.

Although the microbial data clearly support the potential for dissimilatory manganese reduction in the intermediate-salinity zone, alternative pathways for manganese oxide reduction need to be evaluated. Potential inorganic reductants for manganese oxide phases include dissolved sulfide, Fe(II), and ammonium.

Measurable levels of dissolved sulfide are found at salinities as low as 130‰ (Figure 4E). Thus, reaction with sulfide could potentially be responsible for reduction of manganese oxide phases (*26*). A simplified representation of the overall stoichiometry of this pathway is

$$MnO_2 + H_2S + 2H^+ \rightarrow Mn^{2+} + 2H_2O + S^0 \quad (2)$$

Reaction 2 produces a stoichiometric ratio of alkalinity to Mn^{2+} generation similar to that of dissimilatory Mn reduction (2:1). However, the maximum deviation of the total dissolved H_2S concentration from conservative mixing amounts to only $\sim$12 μM (Figure 4E). Thus, it would appear that reaction

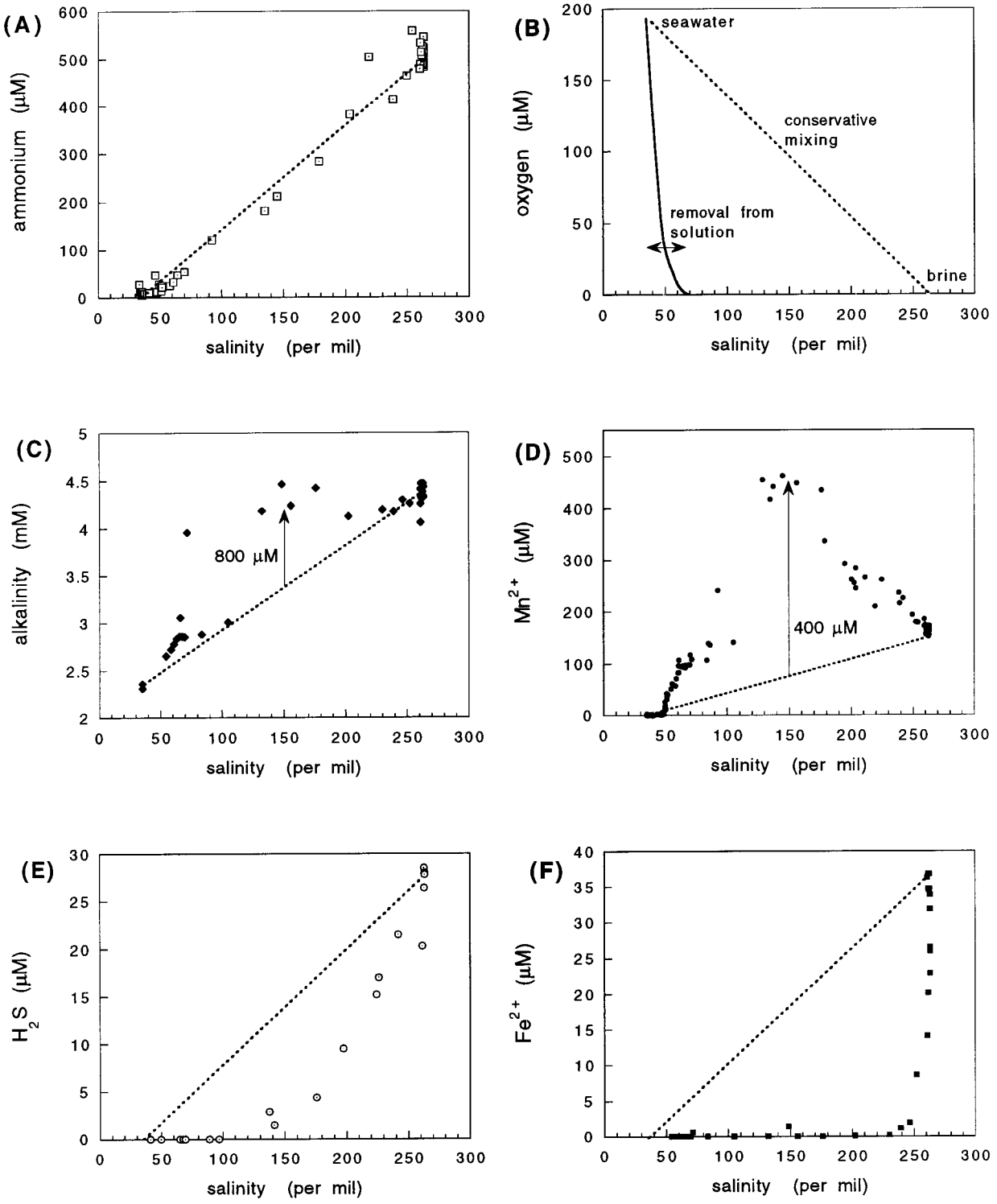

FIGURE 4. Mixing diagrams of ammonium (A), O_2 (B), total alkalinity (C), dissolved Mn^{2+} (D), dissolved H_2S (E), and dissolved Fe^{2+} (F). Broken lines represent conservative mixing. Vertical arrows on (C) and (D) show the magnitudes of excess alkalinity and Mn^{2+} production (see text for discussion).

with dissolved sulfide can account only for a small fraction (≤3%) of the observed production of Mn^{2+}. This conclusion assumes that no significant amount of sulfide is being produced at salinities <180‰. That is, it assumes that bacterial sulfate reduction becomes an important pathway for organic matter degradation only after most of the bioavailable manganese oxides have been reduced (*27*).

Reaction with dissolved Fe(II) offers another possible reduction pathway for manganese oxides (*28*). However, it cannot explain the large production of Mn^{2+} in the salinity region 60−180‰ either. The mixing diagram of dissolved Fe(II) (Figure 4F) shows that reactions consuming Fe(II) ions are restricted to the high-salinity region of the transition zone (>200‰). Furthermore, as for H_2S, the maximum removal of Fe(II), relative to the conservative mixing line, could explain only a minor portion of the observed buildup of dissolved Mn(II).

Reaction with ammonium has recently been proposed as a possible reduction mechanism for manganese oxides in marine sediments (*29*):

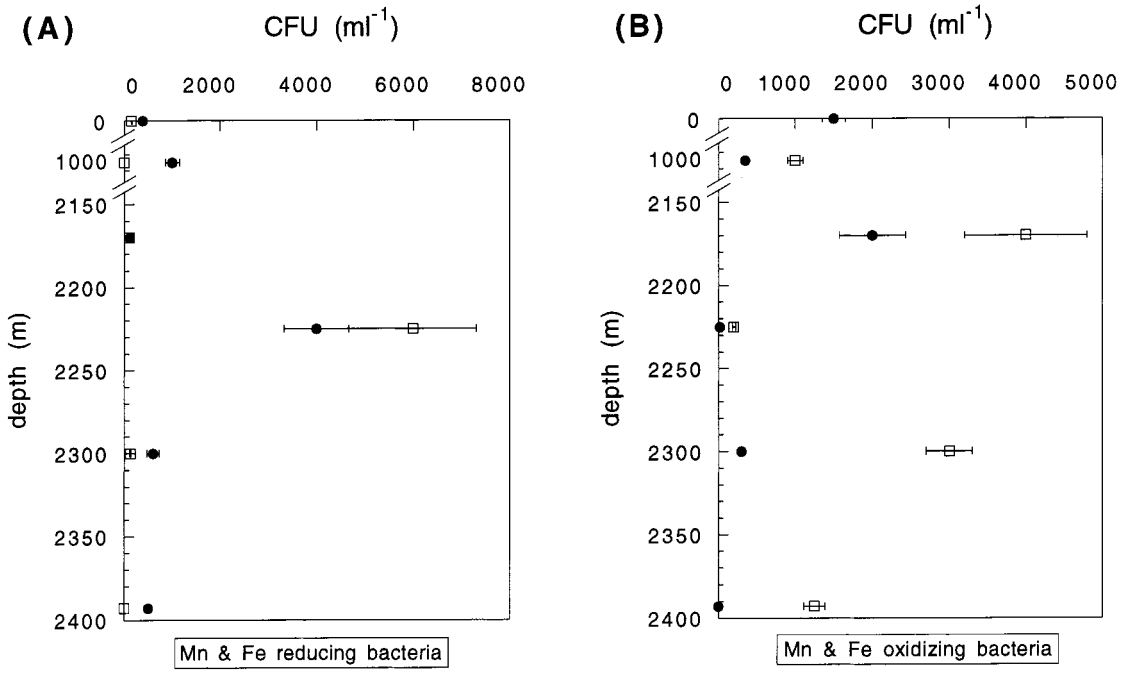

FIGURE 5. Depth profiles of bacterial colony forming units (CFU), per milliliter of water sample, grown anaerobically on complex medium with Mn(IV) or Fe(III) as terminal electron acceptor (A) and aerobically on B1 medium with Mn(II) or Fe(II) as electron donor (B): (open squares) Mn-reducing and Mn-oxidizing bacteria; (solid circles) Fe-reducing and Fe-oxidizing bacteria. Note the compressed depth scale at top of the graphs. See text for complete discussion.

$$3MnO_2 + 2NH_3 + 6H^+ \rightarrow 3Mn^{2+} + N_2 + 6H_2O \quad (3)$$

If this reaction was an important process generating Mn^{2+}, a large convex-down curvature of the ammonium mixing diagram would be expected. In the salinity range 70−250‰, however, the ammonium concentration closely follows the conservative mixing line (Figure 4A). The curvature in the low-salinity region (<70‰) most likely reflects ammonium oxidation by O_2 (nitrification).

Thus, in view of the cumulative evidence, bacterial respiration with manganese oxides as terminal electron acceptor (reaction 1) appears to be the main reduction pathway of manganese across the redoxcline of the Orca Basin. It is the source of the high dissolved Mn(II) (>400 μM) and alkalinity (>4 mM) levels observed at intermediate salinities, and it represents the dominant pathway of organic matter degradation in the depth range 2210−2240 m.

Manganese oxides reduced in the intermediate salinity region are continuously regenerated in the low-salinity range, 45−52‰ (depth interval 2180−2210 m), as inferred from the convex-down curvature of the Mn^{2+} mixing diagram in the low-salinity region (Figure 4D). The removal of dissolved Mn^{2+} is closely matched by an increase of the particulate Mn concentration by a factor of ~30, within the depth interval 2190−2210 m (Figure 6A). The particulate Mn peak occurs in the salinity range where the total suspended matter concentration remains fairly constant (*9*); therefore, it must represent a transfer of dissolved Mn to the particulate matter. Dissolved O_2 is present in the depth interval 2180−2210 m; hence, the probable reaction consuming Mn^{2+} is

$$2Mn^+ + O_2 + 2H_2O \rightarrow 2MnO_2 + 4H^+ \quad (4)$$

The highest number of CFU of manganese oxidizing bacteria (MOB) was measured at the upper end of the zone of Mn oxygenation (2170 m, Figure 5B). The CFU are ~4-fold more abundant than at 1000 m, where O_2 concentrations are near saturation. This finding suggests that a major fraction of the microbial population at 2170 m consists of MOB that are capable of obtaining energy for aerobic growth by oxidizing Mn(II). This hypothesis is further supported by the low numbers of CFU associated with other members of the microbial community, including aerobic heterotrophs (see above) and the anaerobic MRB (Figure 5A). Thus, the culture data are consistent with a regeneration of manganese oxides via microbial oxygenation, as proposed for a variety of other marine environments (*6*, *30*, *31*). Although bacterial CFU were not enumerated in the depth interval 2180−2210 m, that is, the inferred zone of most intense Mn(II) oxygenation, we expect that the numbers of MOB CFU are even higher in this region than at 2170 m.

The highest number of CFU of iron oxidizing bacteria (FOB) was also measured at sampling depth 2170 m, whereas the number of anaerobic FRB CFU were at correspondingly low levels. However, as discussed below, Fe(II) oxidation is not taking place within the low-salinity range. Thus, although the resident bacterial population is capable of oxidizing both Mn(II) and Fe(II), only the potential for manganese oxidation is being expressed at the top of the transition zone.

The number of MOB CFU decreases dramatically at 2225 m, the depth where the number of (anaerobic) MRB CFU is highest (Figure 5). This observation is not surprising: the absence of O_2 at 2225 m allows the population of MRB, but not MOB, to propagate. The numbers of FOB and FRB CFU show a similar response to the disappearance of O_2 between 2170 and 2225 m. Below a water depth of 2225 m, however, the MOB and FOB CFU show different patterns. The FOB CFU remain relatively low, but the MOB CFU rebound to significant levels. Although the low number of FOB CFU is expected, given the absence of O_2, the abundance of aerobically grown MOB is not so easily explained. It is possible that the observed colony forming Mn oxidizing bacteria have retained the ability to respire aerobically, even though they reside in a permanently anoxic zone of the basin water column. Further efforts to characterize these bacteria, including testing for their terminal electron-accepting capabilities, are currently underway.

Some reactive Mn is continuously lost from the salinity transition zone and is ultimately buried in the sediments.

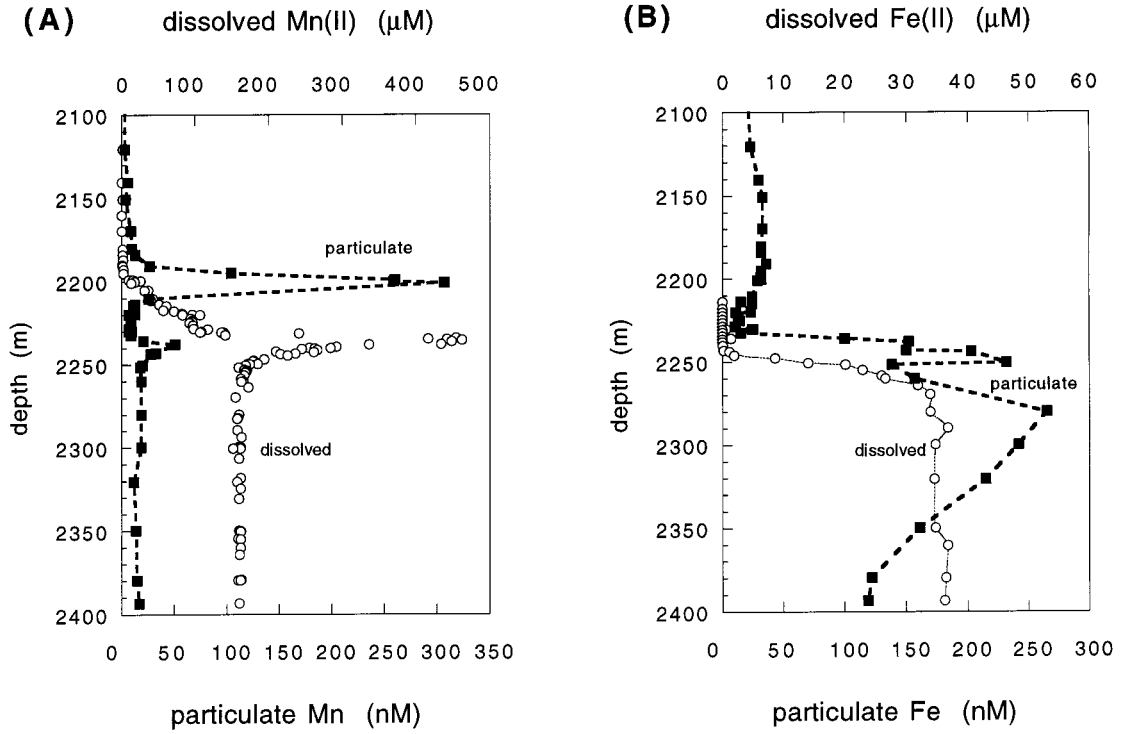

FIGURE 6. Depth profiles of dissolved and particulate manganese (A) and dissolved and particulate iron (B).

TABLE 1. Chemical Composition of Orca Basin Brine

	total molalities
Ca^{2+}	2.90×10^{-2}
Mg^{2+}	4.24×10^{-2}
Na^{+}	4.24×10^{-0}
K^{+}	1.70×10^{-2}
Fe^{2+}	3.71×10^{-5}
Mn^{2+}	2.12×10^{-4}
Cl^{-}	4.45×10^{-0}
SO_4^{2-}	2.90×10^{-2}
HCO_3^{-}	4.74×10^{-3}
total alk	4.77×10^{-3}
pH 6.5	temp = 5 °C
$I = 4.57$	

Given the high levels of alkalinity (Figure 4C) and dissolved Mn(II) (Figures 4D and 6A) in the high-salinity region and the brine itself, in situ precipitation of manganese carbonate

$$Mn^{2+} + HCO_3^{-} \rightarrow MnCO_3 + H^{+} \qquad (5)$$

has been proposed as a pathway through which reactive manganese is transferred to the sediments (*9*, *32*). Chemical extractions performed on sediments from the deepest portion of the Orca Basin suggest that Mn is indeed largely associated with the carbonate fraction (*32*).

Because reaction 5 is reversible, the brine solution should approach equilibrium with respect to the authigenic manganese carbonate phase. The average brine composition, compiled from our own plus published (*10*, *14*) data, is listed in Table 1. Equilibrium calculations were performed with the computer program PHRQPITZ (*33*), which uses Pitzer's equations (*34*) to correct for strong ion interactions in the brine. Published values of the solubility product K_s of rhodocrosite range from $10^{-11.05}$ for well-crystallized $MnCO_3$ to $10^{-10.39}$ for synthetic $MnCO_3$ (*35*). For this range of K_s, the saturation index with respect to $MnCO_3$, SI = $\log(IAP/K_s)$ with IAP = $(Mn^{2+})(CO_3^{2-})$, varies between 0.1 and −0.5. That is, the brine appears to be reasonably close to equilibrium with $MnCO_3$; thus, the stable dissolved Mn(II) concentration in the brine (Figure 6A) could be controlled by the solubility of authigenic manganese carbonate.

The mixing diagram of Mn^{2+} does not show a pronounced convex-down curvature in the high-salinity region (Figure 4D), as would be expected if reaction 5 was a very efficient removal mechanism of Mn(II). Thus, while most Mn ions cycle through their reduced dissolved and oxidized particulate forms in the salinity transition zone, apparently only a small fraction of the ions escapes and settles into the brine. This is consistent with the relatively low concentrations of Mn measured in particulate matter from the brine pool (Figure 6A) and in the underlying sediments (*32*).

A comparison of the depth distributions of iron and manganese (Figure 6) shows that dissolved Fe(II) concentrations increase below the maximum of dissolved Mn(II). The highest levels of dissolved Fe^{2+} are found within the brine itself. As the Fe^{2+} ions diffuse out of the brine, they are rapidly consumed in the salinity range 230−260‰ (Figure 4F). The disappearance of dissolved Fe roughly coincides with a local maximum of the concentration of solid-bound Fe between 2230 and 2250 m (salinity range 200−260‰) (Figure 6B). The interpretation of the particulate Fe distribution, however, is complicated by the variability of the concentration of total suspended matter in the region of strongest stratification (see above). That is, both a solution-to-particulate transfer of Fe and an increase of the concentration of total suspended matter may contribute to the observed particulate Fe concentration maximum (*9*).

In most water column studies, the removal of upward transported dissolved Fe(II) is attributed to reaction with O_2, resulting in the precipitation of ferric oxyhydroxides (*1*). However, oxygenation of Fe(II) is not a feasible pathway in the Orca Basin, because a depth interval of >10 m separates nonzero concentrations of O_2 and Fe^{2+}. This can also be seen in the lack of overlap of nonzero concentrations in the mixing diagrams of the two species (Figure 4B,F). Furthermore, bacterial enumeration indicates a near absence of aerobically grown FOB at a depth of 2225 m and below (Figure 5B).

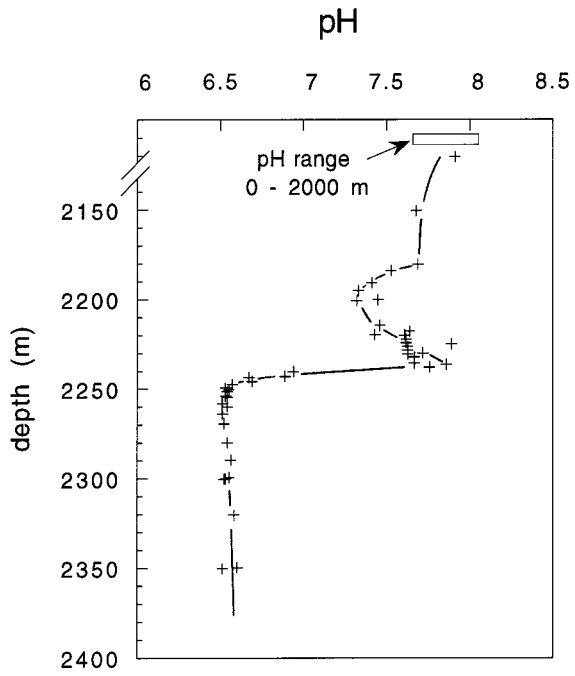

FIGURE 7. Depth profile of pH: fluctuations between water depths of 2180 and 2250 m are interpreted in terms of the major reactions driving the biogeochemical cycle of Mn (see text for discussion).

A possible anaerobic oxidation pathway for dissolved Fe(II) ions is reaction with manganese oxides (*28*):

$$2Fe^{2+} + MnO_2 + 4H_2O \rightarrow 2Fe(OH)_3 + Mn^{2+} + 2H^+ \quad (6)$$

The difficulty with reaction 6 is that it would be taking place in the presence of dissolved sulfide (>5 μM $\sum H_2S$) (Figure 4E). Under these conditions, reaction 6 would compete for manganese oxides with reaction 2. Furthermore, the reaction product, ferric oxyhydroxides, is unstable in the presence of significant levels of dissolved sulfide (*36*).

Alternatively, Fe(II) may be removed by a nonoxidative sorption process. As Fe^{2+} ions diffuse out of the brine pool, they encounter the particles trapped in the lower portion of the salinity transition zone (see above). They also travel along a large pH gradient (Figure 7). The upward increase in particle density as well as the increase in pH would favor adsorption of Fe^{2+} ions to particle surfaces (*1*). Downward settling of particles would in turn regenerate dissolved Fe^{2+}. Unlike the classical model, the sorption−desorption scenario does not involve cycling of Fe between reduced and oxidized states. Further work, including a detailed characterization of particulate Fe speciation (*37*), will be needed to determine whether this hypothetical nonredox cycling is an important mechanism controlling the dissolved and particulate distributions of iron in the Orca Basin.

In sediment cores collected along the basin's margin above the oxycline, we observed core sections with a strong red coloration, indicative of authigenic iron(III) oxyhydroxides (X-ray diffraction revealed the presence of hematite). Thus, in addition to possible in situ production via reaction 6, settling of land-derived detritus or lateral sediment transport may supply reactive iron(III) oxyhydroxides to the salinity transition zone. However, even if a significant fraction of the particulate Fe maximum in the 2230−2250 m depth range is composed of bioavailable iron(III) oxyhydroxides, dissimilatory iron reduction would be limited by the presence of relatively high levels of dissolved sulfide. Rapid reduction by sulfide would effectively outcompete the utilization of the reactive iron(III) oxyhydroxides by FRB (*3*).

The presence of detectable dissolved sulfide (Figure 4E) and the absence of significant FRB CFU below a depth of 2225 m (Figure 5A) suggest that bacterial sulfate reduction is the main pathway for organic matter degradation in the high-salinity zone and in the brine pool (depth > 2240 m). The dissolved sulfide produced by sulfate reduction would rapidly react with dissolved iron(II) and iron(III) oxyhydroxides, resulting in the formation of iron sulfides in the water column (*38*). The efficient in situ formation of iron sulfides is consistent with the relatively high concentrations of particulate Fe measured in the brine (compare the particulate Mn and Fe distributions in Figure 6). The observed enrichment in iron sulfides of Orca Basin sediments (*39*) further confirms that precipitation of sulfide phases is the major removal mechanism of reactive Fe from the transition zone.

The depth distributions of the reactions discussed above explain the observed pH profile across the seawater to brine transition (Figure 7). The pH drops by ~0.4 pH unit between 2180 and 2200 m, which corresponds to the depth range where intense Mn^{2+} oxygenation produces H^+ (reaction 4). Subsequently, pH increases by ~0.5 unit to a water depth of 2238 m. This increase can be attributed to H^+ consumption by dissimilatory Mn reduction (reaction 1). Finally, the pH decreases from 7.8 to 6.5 in the depth range 2238−2250 m. This large pH gradient mostly reflects mixing with the low-pH brine. However, a number of the proposed reactions, that is, reactions 5 and 6, adsorption of Fe^{2+} and reaction between Fe^{2+} and sulfide, could also contribute to lowering of the pH just above the brine. Thus, the pH distribution acts as a sensitive indicator of the biogeochemical processes in the salinity transition zone.

In conclusion, the slow rate of escape of Mn ions to the brine and, ultimately, the sediments sustains the efficient redox cycling of Mn ions in the transition zone. In contrast, the cycling of Fe ions is limited by the rapid formation and settling of iron sulfides. As a result, the acid−base chemistry, redox transformations, and microbial metabolic activity within the salinity transition zone are largely controlled by the intense, microbially mediated redox cycle of Mn. Thus, the Orca Basin provides an ideal setting in which to study the behavior and fate of organic matter, nutrients, and metals across a manganese-dominated redoxcline.

Acknowledgments

The captain and crew of the R/V *Longhorn* are thanked for their assistance. The constructive criticisms and suggestions of the Guest Editor and three Journal reviewers helped improve the manuscript. Financial support for this project was provided by the National Science Foundation (OCE-9415563, EAR-9708535), the Office of Naval Research (N00014-95-1-0206), and the U.S. Environmental Protection Agency (R-825397).

Literature Cited

(1) Stumm, W.; Morgan, J. J. *Aquatic Chemistry*; Wiley: New York, 1996.
(2) Davison, W. *Earth-Sci. Rev.* **1993**, *34*, 119−163.
(3) Wang, Y.; Van Cappellen, P. *Geochim. Cosmochim. Acta* **1996**, *60*, 2993−3014.
(4) Friedl, G.; Wehrli, B.; Manceau, A. *Geochim. Cosmochim. Acta* **1997**, *61*, 275−290.
(5) Appelo, C. A. J.; Postma, D. *Geochemistry, Groundwater and Pollution*; A. A. Balkema: Rotterdam, 1993.
(6) Tebo, B. M.; Emerson, S. *Appl. Environ. Microbiol.* **1985**, *50*, 1268−1273.
(7) Stumm, W.; Sulzberger, B. *Geochim. Cosmochim. Acta* **1992**, *56*, 3233−3257.
(8) DiChristina, T. J.; DeLong, E. F. *Appl. Environ. Microbiol.* **1993**, *59*, 4152−4160.
(9) Trefry, J. H.; Presley, B. J.; Keeney-Kennicutt, W. L.; Trocine, R. P. *Geo-Mar. Lett.* **1984**, *4*, 125−130.

(10) Shokes, R. F.; Trabant, P. K.; Presley, B. J.; Reid, D. F. *Science* **1977**, *196*, 1443−1446.
(11) Imboden, D. M.; Wüest, A. In *Physics and Chemistry of Lakes*; Lerman, A., Imboden, D. M., Gat, J. R., Eds; Springer-Verlag: Berlin, 1995.
(12) Millero, F. J.; Surdo, A. L.; Chetirkin, P.; Guinasso, N. L. *Limnol. Oceanogr.* **1979**, *24*, 218−225.
(13) Wiesenburg, D. A. Geochemistry of Dissolved Gases in the Hypersaline Orca Basin. Ph.D. Thesis, Texas A&M, College Station, TX, 1980.
(14) Sackett, W. M.; Brooks, J. M.; Bernard, B. B.; Schwab, C. R.; Chung, H.; Parker, R. A. *Earth. Planet. Sci. Lett.* **1979**, *44*, 73−81.
(15) Dickson, A. G. *Deep-Sea Res.* **1993**, *40*, 107−118.
(16) Ben-Yaakov, S.; Sass, E. *Limnol. Oceanogr.* **1977**, *22*, 374−376.
(17) Sarazin, G.; Michard, G.; Prevot, F. *Water Res.* In press.
(18) Stookey, L. L. *Anal. Chem.* **1970**, *42*, 779−781.
(19) Strickland, J. D. H.; Parsons, T. R. *A Practical Handbook of Sea Water Analysis*; Queen's Printer: Ottawa, 1968.
(20) Parsons, T. R.; Maita, Y.; Lalli, C. M. *A Manual of Chemical and Biological Methods for Seawater Analysis*; Pergamon: Oxford, U.K., 1984.
(21) Meyers, C. R.; Nealson, K. H. *J. Bacteriol.* **1990**, *172*, 6232−6238.
(22) DiChristina, T. J.; DeLong, E. F. *J. Bacteriol.* **1994**, *176*, 1468−1474.
(23) Lovley, D. R.; Phillips, E. J. P. *Appl. Environ. Microbiol.* **1988**, *54*, 1472−1480.
(24) Hanert, H. H. In *The Prokaryotes*; Balows, A., Ed.; Springer-Verlag: New York, 1992.
(25) Liss, P. S. In *Estuarine Chemistry*; Burton, J. D., Liss, P. S., Eds.; Academic Press: New York, 1976.
(26) Yao, W.; Millero, F. J. *Geochim. Cosmochim. Acta* **1993**, *57*, 3359−3365.
(27) Canfield, D. E.; Thamdrup, B.; Hansen, J. W. *Geochim. Cosmochim. Acta* **1993**, *57*, 3867−3883.
(28) Postma, D. *Geochim. Cosmochim. Acta* **1985**, *49*, 1023−1033.
(29) Luther III, G. W.; Sundby, B.; Lewis, B. L.; Brendel, P. J.; Silverberg, N. *Geochim. Cosmochim. Acta* **1997**, *61*, 4043−4052.
(30) Sunda, W. G.; Huntsman, S. A. *Limnol. Oceanogr.* **1987**, *32*, 552−564.
(31) Tebo, B. M.; Rosson, R. A.; Nealson, K. H. In *Black Sea Oceanography*; Izdar, E., Murray, J. W., Eds.; Kluwer: Dordrecht, 1991.
(32) Sheu, D.-D. The Geochemistry of Orca Basin Sediments. Ph.D. Thesis, Texas A&M, College Station, TX, 1983.
(33) Plummer, L. N.; Parkhurst, D. L.; Fleming, G. W.; Dunkle, S. A. U.S. Geol. Surv. Water Res. Inv. Report 88-4153; Reston, VA, 1988.
(34) Pitzer, K. S. In *Thermodynamic Modeling of Geological Materials: Minerals, Fluids and Melts*; Carmichael, I. S. E., Eugster, H. P., Eds.; Mineral. Rev. 17; Mineralogical Society of America: Washington, DC, 1987.
(35) Nordstrom, D. K.; Plummer, L. N.; Langmuir, D.; Busenberg, E.; May, H. M. In *Chemical Modeling of Aqueous Systems II*; Melchior, D. C., Bassett, R. L., Eds.; ACS Symposium Series 416; American Chemical Society: Washington, DC, 1990.
(36) Canfield, D. E.; Raiswell, R.; Bottrell, S. H. *Am. J. Sci.* **1992**, *292*, 659−683.
(37) Lienemann, C.-P.; Taillefert, M.; Perret, D.; Gaillard, J.-F. *Geochim. Cosmochim. Acta* **1997**, *61*, 1437−1446.
(38) Canfield, D. E.; Lyons, T. W.; Raiswell, R. *Am. J. Sci.* **1996**, *296*, 818−834.
(39) Sheu, D.-D.; Presley, B. J. *Mar. Geol.* **1986**, *70*, 103−118.

Received for review March 27, 1998. Revised manuscript received June 1, 1998. Accepted June 15, 1998.

ES980307M